Composites Part B 185 (2020) 107782

Contents lists available at ScienceDirect

Composites Part B

journal homepage: www.elsevier.com/locate/compositesb

Rapid synthesis of solid amine composites based on short mesochannel SBA-15 for CO_2 capture

Beibei Ma [a], Rijia Lin [b], Hui He [a], Qinghua Wu [a], Shuixia Chen [a,c,*]

[a] PCFM Lab, School of Chemistry and Chemical Engineering, Sun Yat-Sen University, Guangzhou, 510275, PR China
[b] School of Chemical Engineering, The University of Queensland, Brisbane, Queensland, 4072, Australia
[c] Materials Science Institute, Sun Yat-Sen University, Guangzhou, 510275, PR China

ARTICLE INFO

Keywords:
Short mesochannel SBA-15
Non-hydrothermal
$NH_3{\cdot}H_2O$ catalysis
CO_2 adsorption
Adsorption kinetics

ABSTRACT

Hydrothermal is common process for synthesizing well-ordered mesoporous silica, however, it costs time and energy simultaneously. To improve the efficiency of synthesis process, it is necessary to propose a facile synthesis strategy with less time and energy requirement. In this study, an innovative non-hydrothermal method using $NH_3{\cdot}H_2O$ as catalyst after ripening step is developed to prepare SBA-15 with short mesochannels (SSBA-15) for the first time. The synthesis period of SSBA-15 framework was extremely shortened within 40 min under the optimized conditions (30 min of ripening step and 25% of $NH_3{\cdot}H_2O$ concentration), while obtained material exhibits well-ordered hexagonal pore structure and fine particle morphology of SSBA-15 (pore length of 250 ± 50 nm and mesopore size of 9.8 nm). This method can also be employed to synthesize conventional SBA-15 successfully. Moreover, the application of SSBA-15 as support of solid amine adsorbents on CO_2 adsorption and well-fitting of experimental CO_2 adsorption data with Avrami and intraparticle diffusion models reveal that the adsorbents combine the advantages of micro-mesoporous structure, short mesochannel and amine reagents (high affinity of CO_2), resulting in enhanced molecular diffusion, fast adsorption kinetics and high CO_2 adsorption capacity. Notably, the solid amine adsorbents exhibited excellent regeneration ability during ten adsorption-desorption cycles. This work opens up new opportunities in efficient preparation of materials that require hydrothermal process.

1. Introduction

Since the first report of ordered mesoporous silica (M41S family) in the early 1990s [1], the researches focused on mesoporous silica became more and more popular on account of its designable particle morphology and porous structure, which is vital when being utilized as support of composites for various applications [2–4]. As nanocarrier, SBA-15 type of mesoporous silica with unique micro-mesoporous structure [5] has better hydrothermal stability [6], mass transfer rate [7] and controllable adsorption and release of active substance [8], making it attractive among worldwide researchers and in diverse range of application fields, such as drug delivery [9,10], environmental protection [11,12], CO_2 adsorption [13,14] and catalysis research [15–19]. The tunable structure of SBA-15 (pore length, pore size and channel structure) has been realized by adjusting the synthesis system, for instance, introduction of alkanes, inorganic electrolytes, mental irons and swelling agent [20–23], yet the synthesis period remained energy costing because of the requirement of time and temperature for hydrothermal process [24–26]. In order to reduce the synthesis time, microwave irradiation, as an energy efficient and environmentally friendly technology, has been applied in synthesis of ordered mesoporous silicas to provide rapid and homogeneous heating for the synthesis system, accelerate rates of reactions, and benefit formation of uniform nucleation centers [27–29]. Among published researches, microwave-assisted hydrothermal process can only reduce the synthesis period to 4 h (ripening for 2 h and microwave-assisted hydrothermal treating for 2 h) [30] to obtain good-quality SBA-15, even when the entire synthesis process (ripening period at low-temperature and aging period under hydrothermal treatment) was under microwave irradiation, it still costs at least 3 h to form a well-ordered framework [31].

Considering that SBA-15 is synthesized under acid conditions, we propose using $NH_3{\cdot}H_2O$ to promote the synthesis of mesoporous silica.

* Corresponding author. PCFM Lab, School of Chemistry and Chemical Engineering, Sun Yat-Sen University, Guangzhou, 510275, PR China.
E-mail addresses: mabeibei555@163.com (B. Ma), r.lin1@uq.edu.au (R. Lin), guizhouhehui@163.com (H. He), wqh107abc@163.com (Q. Wu), cescsx@mail.sysu.edu.cn (S. Chen).

https://doi.org/10.1016/j.compositesb.2020.107782
Received 11 December 2019; Received in revised form 15 January 2020; Accepted 15 January 2020
Available online 20 January 2020

As being reported by many researchers, $NH_3{\cdot}H_2O$ has been applied in many synthesis systems, for example, sol-gel system [32,33], electrolyte system [34] and emulsion liquid membrane [35], and shows remarkably favorable influences, especially in sol-gel systems, the skeleton structures and pore sizes change with the adjustment of $NH_3{\cdot}H_2O$ concentration [33]. Furthermore, the morphology of SBA-15 particles has significant impact on the adsorption processes. It has been proven that short mesochannel SBA-15 is more favorable for mass transfer compared with conventional SBA-15, which leads to faster adsorption rate and higher adsorption capabilities in the applications on adsorption [36,39]. Herein, we report a facile strategy abolishing hydrothermal process, instead, using $NH_3{\cdot}H_2O$ as catalyst to promote the polycondensation of P123-TEOS precursor aggregations after ripening step (Fig. 1), which can sharply shorten the synthesis period and successfully obtain well-ordered hexagonal SBA-15 with short mesochannels. The optimal synthesis condition was explored by adjusting ripening time and $NH_3{\cdot}H_2O$ concentration. Subsequently, the CO_2 adsorption properties of solid amine adsorbents based on as-prepared SSBA-15 were evaluated by regeneration ability and CO_2 adsorption capacity under various temperatures. Moreover, investigations on the kinetics and diffusion models were carried out to have further insights into the influence of SSBA-15 support on the adsorption process, rate-controlling step and diffusion mechanism.

2. Experimental

2.1. Chemicals

Triblock copolymer P123 (Sigma-Aldrich, China), tetraethyl orthosilicate (TEOS, Aladdin chemistry, China), decane (98%, Aladdin chemistry, China) and polyethyleneimine (PEI, >99%, Aladdin chemistry, China) were used directly. NH_4F (AR), HCl (37%) and $NH_3{\cdot}H_2O$ (25%) were provided by Guangzhou Chemical Reagent Factory, China.

2.2. Preparation of SSBA-15

The synthesis of SSBA-15 in this work was mainly parted into two processes: 1) the aggregating of P123-TEOS precursors, 2) the polycondensation of aggregation via catalysis of $NH_3{\cdot}H_2O$. A typical preparation in the first process was similar to reported literature [30]. In brief, the mixture of 4.0 g of P123, 140 mL of HCl solution (1.6 M), 8.8 g of TEOS, 23.3 g of decane and 0.041 g of NH_4F at 40 °C was stirred for given time (2 min, 4 min, 6 min, 10min and 30min). Subsequently, $NH_3{\cdot}H_2O$ was added dropwise to adjust the pH value of the synthesis system to 7–8 (tested by pH test strips) under room temperature (around 25 °C). The products denoted as SSBA-15-*t*-c, in which *t* stands for ripening time, and *c* stands for the weight percentage of $NH_3{\cdot}H_2O$, were obtained by filtration, air-drying (80 °C) and then calcination (550 °C) for 3 h in a furnace for template removal.

2.3. Preparation of SSBA-15 based solid amine adsorbents

The solid amine adsorbents were prepared by impregnating amine reagents, PEI (M_w = 600, 1800, 10,000) and hyperbranched polyamine prepared by our research group [37] (HBP(DETA), HBP(TETA), HBP (TEPA), the possible structure of HBP is shown in Fig. S1, Supplementary Information) into as-prepared SSBA-15. The specific procedure was as follows: 1 g amine reagent was solved completely in 10 mL ethanol under 70 °C, followed with the addition of 1 g as-prepared SSBA-15 and another 10 mL ethanol, then the mixture was stirred for 5 h. After finely dispersing, the mixed solid was collected by centrifugation (10,000 r/min, 20 min), dried at 80 °C. The prepared solid amine adsorbents were named as SSBA-15-PEI(x) or SSBA-15-HBP(y), where *x* represents for the molecular weight of PEI and *y* stands for DETA, TETA or TEPA.

2.4. Characterization

ASAP2020 (Micromeritics Corp, USA) was used to test porous parameters of obtained samples by measuring adsorption-desorption isotherms of N_2 (77.35 K) and calculating S_{BET} and pore diameter distribution. The morphology and porous structure were analyzed by scanning electron microscope (SEM, S4800, Hitachi, Japan) and transmission electron microscope (TEM, JEM-2010HR, JEOL, Japan). The ordered hexagonal mesoporous structures were identified by Small-

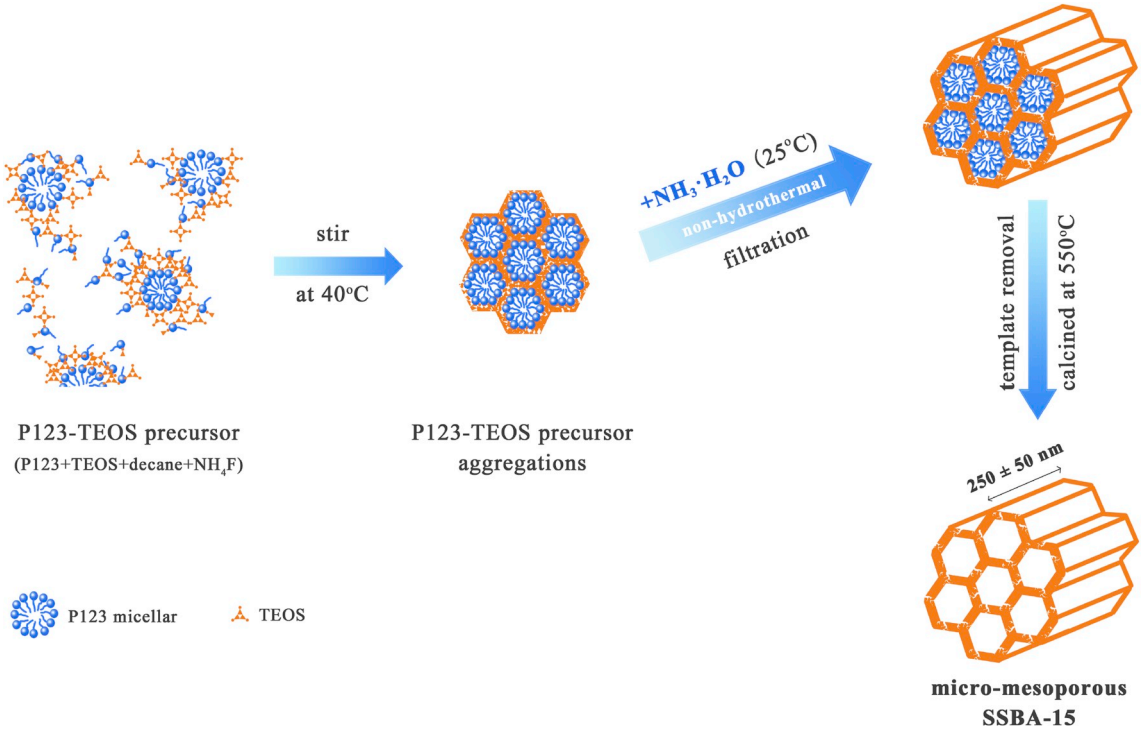

Fig. 1. Schematic diagram of the synthesis of SSBA-15 via non-hydrothermal strategy.

angle X-ray diffraction (SAXD, D8 ADVANCE, BRUKER Textile Technologies GmbH & Co., KG, Germany) in angle with 2θ between 0.50° and 2.5°. Elemental analysis (EA, Analysen systeme GmbH Elementar Vario EL, Germany) was employed to estimate the contents of N, C and H of the solid amine adsorbents.

2.5. CO_2 adsorption process

This CO_2 adsorption-desorption process was carried out in a fixed adsorption column ($\Phi = 1.3$ cm) padded with 0.5 g of adsorbent powder. Residue water and air in the adsorption column were removed by introducing dry N_2 flow (30 mL/min) at 90 °C into the adsorption column for 10 min. Then the CO_2 adsorption test started with dry gas mixture of CO_2/N_2 (with molar ratio of 1:4) at a flow rate of 30 mL/min under the temperature ranging from 0 °C to 90 °C (0 °C, 15 °C, 30 °C, 45 °C, 60 °C, 75 °C, 80 °C, 85 °C, 90 °C), and we detected the outlet concentration of CO_2 every minute by gas chromatograph (Agilent 6820) equipped with a thermal conductivity detector. For followed CO_2 desorption, the adsorbents were regenerated with dry N_2 flow under 90 °C.

3. Results and discussion

3.1. Preparation of SSBA-15 and characterization

Numbers of mesoporous silica have been prepared by stirring at low temperature for different time and catalyzing with different $NH_3 \cdot H_2O$ concentrations. To prove the as-prepared material have well-ordered hexagonal mesoporous structure of SBA-15, characterizations on SEM, TEM, SAXD and N_2 adsorption-desorption were carried out. It was obvious that the sample particles were cuboid-like from SEM images (Fig, 2). The extension of the ripening step (stirring at 40 °C) contributes to the clarity of the sample particles when under a particular concentration of $NH_3 \cdot H_2O$ (Fig. 2c, f, and i), since the stability of the P123-TEOS precursor aggregation is mainly affected by the ripening time. In a conventional synthesis of SBA-15, the particle morphology is determined by ripening process, therefore, samples prepared with same ripening duration are lack of variation [38]. However, in this non-hydrothermal method, which used $NH_3 \cdot H_2O$ as catalyst instead, when the ripening time reached certain length (>10min), the morphology of the sample particles obtained via same ripening time can be various under the different concentrations of $NH_3 \cdot H_2O$ used to adjust the pH value of the synthesis system. Noticeably, the dispersibility and uniformity of the sample particles improved with the rise of the $NH_3 \cdot H_2O$ concentration (Fig. 2g, h and i), as $NH_3 \cdot H_2O$ with relatively high concentration can accelerate the polycondensation inside the stable P123-TEOS precursor aggregation, leading to less inter condensation between aggregations, which benefit the formation of short mesochannels of silica particles. Meanwhile, TEM images of SSBA-15-30-25% particles distinctly showed the ordered hexagonal mesoporous structure with the mesochannel length of 250 ± 50 nm (Fig. 3a), which was about half of that of the SBA-15 obtain via microwave-hydrothermal method (450 ± 50 nm) [30], and structural mesopore size around 10 nm (Fig. 3b).

Furthermore, the Small-angle X-ray diffraction patterns (Fig. 4a) of the samples prepared with different synthesis conditions showed several

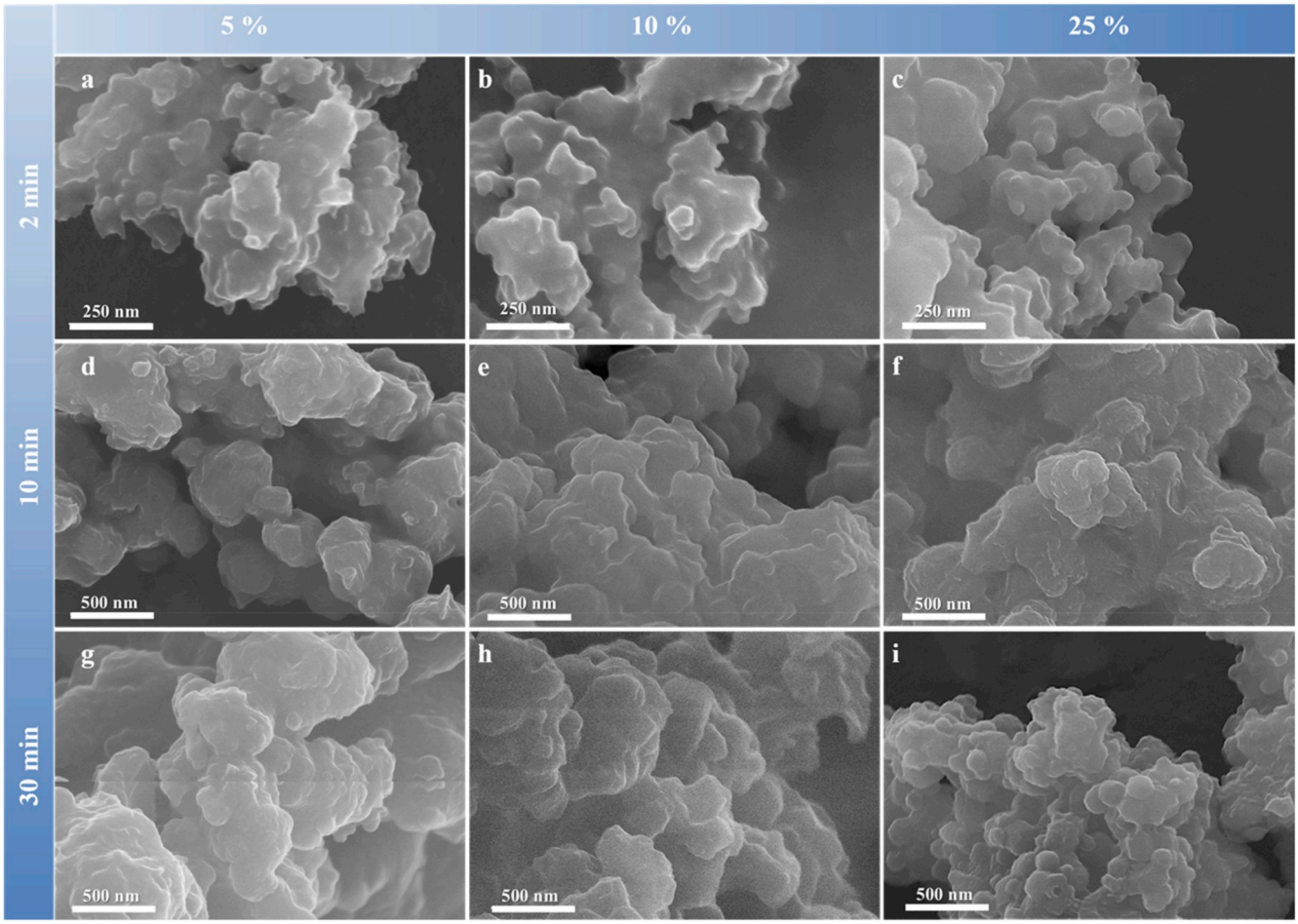

Fig. 2. Scanning electron micrographs of SSBA-15 particles prepared via different ripening time and $NH_3 \cdot H_2O$ concentration. (a. SSBA-15-2-5%, b. SSBA-15-2-10%, c. SSBA-15-2-25%, d. SSBA-15-10-5%, e. SSBA-15-10-10%, f. SSBA-15-10-25%, g. SSBA-15-30-5%, h. SSBA-15-30-10%, i. SSBA-15-30-25%).

peaks that could ascribed to (100), (110) and (200) diffractions, which are the characteristic peaks of highly ordered SBA-15 silica [39]. The above characterizations and discussions demonstrated that well-ordered SBA-15 with short mesochannels was successfully synthesized without hydrothermal process.

3.2. Effects of synthesis conditions on the porous structure of SSBA-15

With respect to the preparation of SSBA-15, the effects of synthesis conditions were focused on ripening time and $NH_3 \cdot H_2O$ concentration. Ripening time was studied by modulating the duration of stirring process from 2 min to 30 min, due to the fact that white precipitation which is the sign of the gathering and orienting of P123-TEOS precursors [40] started to form when stirring time reached 2 min. As shown in Fig. 4b and c, all the samples exhibited the type IV adsorption isotherms, indicating the capillary condensation of mesopores during the N_2 adsorption-desorption procedure [41]. Meanwhile, nitrogen adsorption amount showed a steep increase when $P/P0 < 0.05$, which could be attributed to the massive micropores in the samples.

The hysteresis loops of the N_2 adsorption-desorption isotherms showed the tendency from H3 to H1 while the concentration of $NH_3 \cdot H_2O$ remained the same (Fig. 4b). For the samples prepared under 2 min of ripening time (Fig. S3a, Supplementary Information), the H3 hysteresis loops indicated that these samples obtained through short duration of ripening step were piled up by platelet-like particles, which was consistent with the morphology of particles in SEM images (Fig. 2a, b and c). When the ripening time reached 30 min, the H1 hysteresis loops showed (Fig. S3e, Supplementary Information), proving the formation of ordered mesopores. The pore size distribution became more ordered with the increase of the ripening time. The samples prepared through relatively short ripening time (<10 min), for example, 2 min, had a wide range of pore size from 0.5 nm to 100 nm, including micropores, mesopores and macropores (Fig. S3b, Supplementary Information). Pore size distribution of the samples prepared through relatively long time (>10 min) became narrower and was mainly around 1 nm–2 nm and 10 nm (Figs. S3d and f, Supplementary Information), which were the intrawall micropores and primary mesopores of SSBA-15, respectively.

When the ripening time remained the same, the N_2 adsorption-desorption isotherms of the samples, however, got closer to X axis at lower pressure with the increase of $NH_3 \cdot H_2O$ concentration (Fig. S3 a, c and e, Supplementary Information), indicating the decrease of micropores, which was similar to the results of pore size distribution (Fig. S3 b, d and f, Supplementary Information). With the relatively short ripening time, the increase of $NH_3 \cdot H_2O$ concentration could adjust the pH value of the synthesis system to 7–8 more quickly, leading to a faster condensation between TEOS, which resulted in increased dehydration of PEO segments in silica walls and brought about densification of SSBA-15 framework, namely less intrawall micropores in the samples. Yet the influence of the concentration of $NH_3 \cdot H_2O$ became slight when the ripening time was long enough, which in this case was 30 min, as the duration was long enough to form relatively stable P123-TEOS precursors aggregations and SSBA-15 framework.

Moreover, the improvement of the ordering of these obtained samples, caused by the extension of ripening time and the increase of $NH_3 \cdot H_2O$ concentration, could also be proved by the enhancement of characteristic peak, (100) diffraction, in Small-angle X-ray diffraction patterns (Fig. S2, Supplementary Information). In general, we can confirm that $NH_3 \cdot H_2O$ concentration has a greater impact on the pore structure, the BET surface area and average pore size (Table S1, Supplementary Information) when the ripening time is relatively short (<10 min), while it effects the morphology of the SSBA-15 particles more significantly when the ripening time is relatively long (>10 min). Considering about time and energy saving, 30 min of ripening step and 25% of $NH_3 \cdot H_2O$ concentration is a proper choice for this non-hydrothermal method to prepare SSBA-15 with fine particle morphology and well-ordered pore structure, and the obtained SSBA-15 under optimized condition in TEM image exhibited pore length of 250 ± 50 nm (Fig. 3a) and structural mesopore size of 9.8 nm (Figs. 3b, and Fig. 4c). Surprisingly, the whole process to form a well-ordered framework of SSBA-15 completed within 40 min (30 min of ripening and a few minutes to adjust the pH value of the synthesis system by $NH_3 \cdot H_2O$), which was extremely short when compared with conventional hydrothermal [25] and microwave-hydrothermal [30,31] process.

Furthermore, we verified the applicability of this non-hydrothermal strategy to prepare conventional SBA-15 by leaving out the addition of NH_4F which plays important role in shortening the pore length [30] to the synthesis system. After 24 h of ripening time and been catalyzed by 25% of $NH_3 \cdot H_2O$ concentration, the mesoporous silica consisted of micron scale particles with mesochannel length between 10 μm and 15 μm was obtained (Fig. S4, Supplementary Information), and subsequently characterizations on N_2 adsorption-desorption tests and small-angle X-ray diffraction(Fig. S5, Supplementary Information) indicated that this method prepared conventional SBA-15 successfully. More promisingly, the catalysis of $NH_3 \cdot H_2O$ could be an innovative replacement in preparation of other materials which require hydrothermal process.

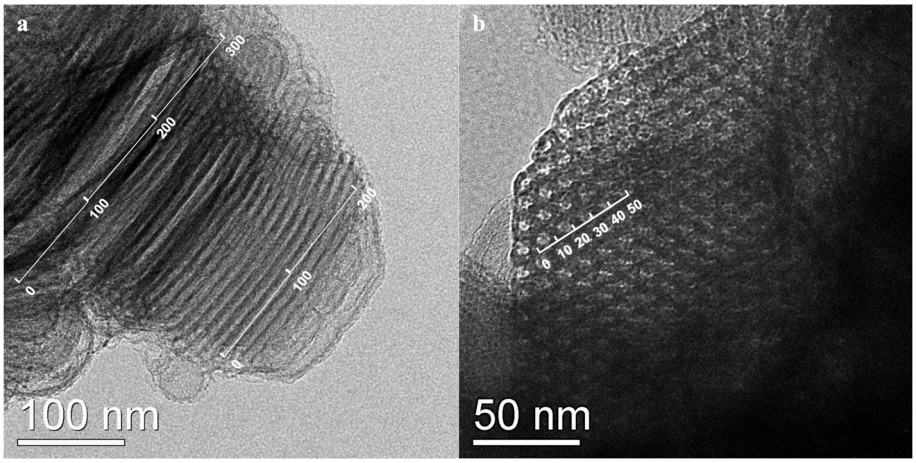

Fig. 3. Transmission electron micrograph of as-prepared SSBA-15-30-25% particles. (a. mesochannel length, b. pore diameter).

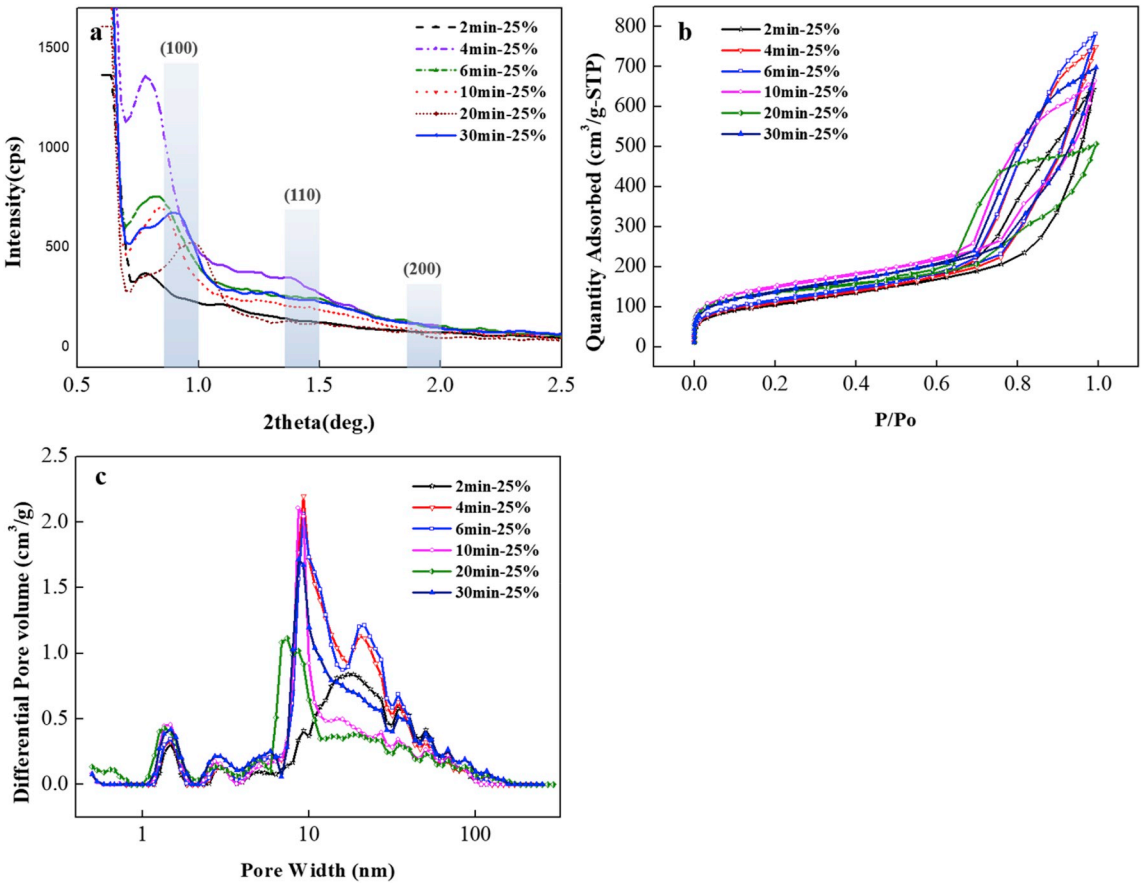

Fig. 4. a) SAXD patterns, b) N_2 adsorption-desorption isotherms at 77 K, and c) pore size distributions of as-prepared SSBA-15 samples.

4. Application in CO_2 adsorption

4.1. CO_2 adsorption properties of SSBA-15 based adsorbents

Being two common functionalization mechanisms of mesoporous matrixes, physical impregnation and chemical grafting have been widely used to prepare the CO_2 adsorbents. Chemical grafting is commonly applied in amination of fibers [42,43], while physical impregnation is employed to prepare solid adsorbents based on porous matrix [26]. We obtained a series of adsorbents with the hyperbranched polyamine prepared by our research group and PEI with different molecular weight via centrifugation-impregnation. The adsorbents impregnated with hyperbranched polymers, especially SSBA-15-HBP (DETA) and SSBA-15-HBP(TETA) had much shorter breakthrough time (Fig. 5a) and much less CO_2 adsorption capacity (Fig. 5b) than the adsorbents impregnated with PEI (Fig. 5, Fig. S6, Supplementary Information), which could be explained as that the amines with small molecular size [36] have lower adhesive force and can be easily tossed out of mesoporous channels under the effect of centrifugal force, resulting in much lower amino density on solid amine adsorbent. Though the CO_2 adsorption tests of SSBA-15-PEI were carried out under dry condition, the abundant Si–OH on the silica walls synergized with primary and secondary amino, resulting in higher CO_2 adsorption capacity ($CO_2 + Si–OH + R_2NH = Si–OH_2^+ + R_2NCOO^-$). Among three adsorbents prepared via impregnating PEI with different molecular weight, SSBA-15-PEI(600) was of the lowest content of N (Table S2,

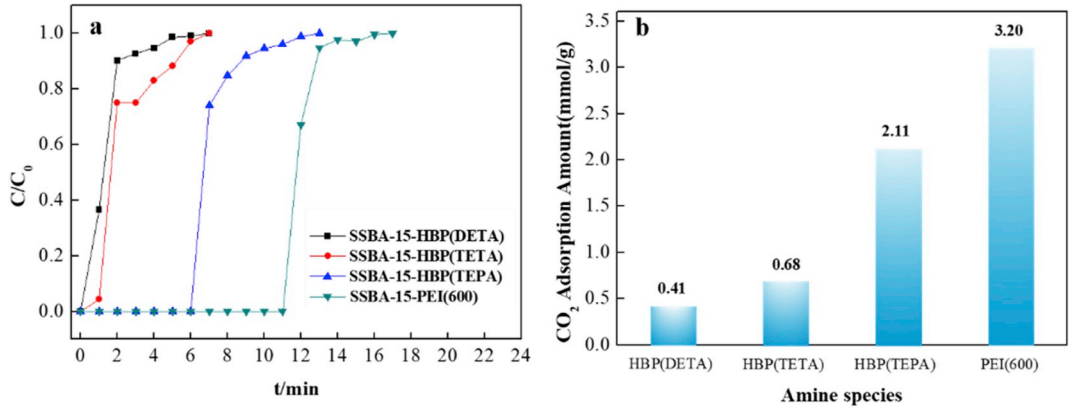

Fig. 5. a) Breakthrough curves of CO_2 adsorption, and b) CO_2 adsorption amounts of as-prepared adsorbents via impregnating different amine species into SSBA-15. (CO_2/N_2 ratio was 1:4; gas flow rate was 30 mL/min; adsorption temperature was 30 °C).

Supplementary Information), yet the highest adsorption amount of CO_2 (3.2 mmol/g at 30 °C, Fig. 5b). That could attributed to the less pore blocking and lower CO_2 transfer resistance, which were fine outcomes of lower viscosity of PEI(600) and its saturated stable loading inside the SSBA-15.

Satisfactorily, the adsorbent based on as-prepared SSBA-15 overcame the shortcomes of adsorbents prepared via impregnation (pore blockage and easily leaching out of amine reagents), and exhibited excellent regenerative ability, which kept stable breakthrough behavior (Fig. 6a) and adsorption amount within integral error (2.11 mmol/g ~ 2.17 mmol/g at 30 °C, Fig. 6b) during 10 times of adsorption-desorption cycles.

As SSBA-15-PEI(600) showed the highest CO_2 adsorption capacity, we focused on studying the detailed thermodynamic properties under different adsorption temperatures with a range from 0 °C to 90 °C. As shown in Fig. 7b, the CO_2 adsorption amount of SSBA-15-PEI(600) increased with the rise of temperature and reached maximum adsorption amount of 4.00 mmol/g under 75 °C, then decreased with further increase of temperature. This result indicated that the CO_2 adsorption behavior of SSBA-15-PEI(600) was governed by both chemical and physical adsorption, otherwise the CO_2 adsorption amount would increase with the decrease of temperature since chemical adsorption of CO_2 is an exothermic process.

4.2. Adsorption kinetics

Three adsorption kinetic models, Pseudo-first order, Pseudo-second order, and Avrami model adopted to fit the experimental data of SSBA-15-PEI(600) at 0 °C–90 °C (Fig. 8, Fig. S7, Supplementary Information) are listed in Eqs. (1) ~ (3), respectively:

$$q_t = q_e\left(1 - e^{-k_f t}\right) \tag{1}$$

$$q_t = q_e \frac{q_e k_s t}{1 + q_e k_s t} \tag{2}$$

$$q_t = q_e\left(1 - e^{(-k_a t)^n}\right) \tag{3}$$

where k_f(min^{-1}), k_s(g mmol^{-1}min^{-1})and k_a (min^{-1}) represent adsorption rate constants, q_e and q_t are the adsorption capacity of the adsorbent at saturated time (when adsorption process approaches equilibrium) and given time, respectively, and n is the kinetic order of the Avrami model.

The experimental data did not fit well with neither Pseudo-first nor Pseudo-second order models (Fig. 8), which overrated the initial adsorption amount and final saturated adsorption amount, underrated the adsorption amount approaching equilibrium, indicating neither of these two kinetic models was suitable for modeling the CO_2 adsorption kinetics of SSBA-15-PEI(600). Meanwhile, the above results indicated that CO_2 adsorption over SSBA-15-PEI(600) is neither simple physical nor simple chemical adsorption [44].

The Avrami model showed well-fitting of the experimental data over the entire adsorption process (Fig. 8), with R^2 ranging from 0.992 to 0.996 and values of q^e calculated from simulation closing to experimental CO_2 adsorption amount (Table S3, Supplementary Information), indicating that Avrami model could fairly correspond to the CO_2 adsorption process of SSBA-15-PEI(600). The fractional order n obtained from Avrami fitting was between 1 and 2 (Table S3, Supplementary Information) which suggested that the synergetic effect of physical and chemical adsorption occurred, and multiple reaction routes appeared. The adsorption rate constants k_a firstly decreases and then increases with an increasing temperature (Table S3, Supplementary Information), demonstrating the adsorption rate reduced and the complete adsorption time prolonged when the temperature was under 80 °C, for example, the breakthrough time at 60 °C,75 °C and 80 °C reached 13 min (Fig. 7a). In fact, kinetics superior in the control of the adsorption at relatively low temperature (<75 °C). The chain segments of PEI(600) tended to be more flexible the kinetic energy of CO_2 molecules enhanced when temperature arises, leading to less resistance in CO_2 diffusion and better exposure of active sites, and resulting in higher CO_2 adsorption amount and lower adsorption rate. However, when the temperature exceeded 75 °C, the equilibrium of adsorption-desorption slightly shifted to desorption under domination of thermodynamics, resulting in mild drop of CO_2 adsorption amount with further increase of temperature.

The cumulative CO_2 adsorption amount under different temperatures demonstrated a two-stage process in saturated adsorption, rapid breakthrough adsorption and gradual approaching equilibrium stage (Fig. 8), in which the equilibrium stage required less time than breakthrough adsorption (Figs. 5a, 6a and 7a), achieving fast complete adsorption. In addition, the proportions of breakthrough adsorption amount in initial stage were over 80% of the saturated adsorption amounts under the temperature ranging from 15 °C to 80 °C (Table S4, Supplementary Information), which is essential for industrial application.

4.3. Diffusion mechanism

Since the CO_2 adsorption is a complex process with all the steps lumped together, Avrami model provided the values to assess adsorption rate, but no outlook in the actual rate-controlling step and the diffusion mechanism of CO_2 adsorption on SSBA-15-PEI(600). Therefore, we analyzed the experimental data by diffusion models showed in Eqs. (4) ~ (7) in order to have further insights into the rate-controlling step and elucidate the CO_2 diffusion mechanism.

Interparticle diffusion model:

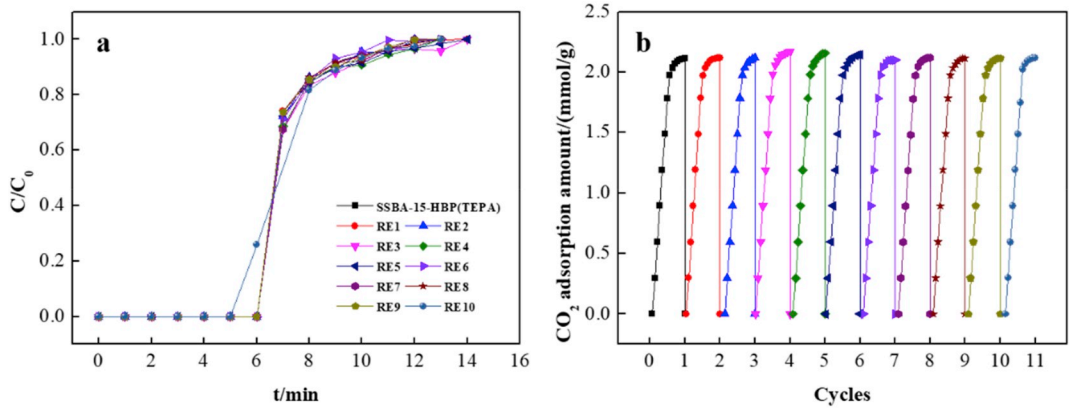

Fig. 6. a) Regenerative breakthrough curves of CO_2 adsorption, and b) recycled CO_2 adsorption-desorption curves.(CO2/N2 ratio was 1:4; gas flow rate was 30 mL/min; adsorption temperature was 30 °C).

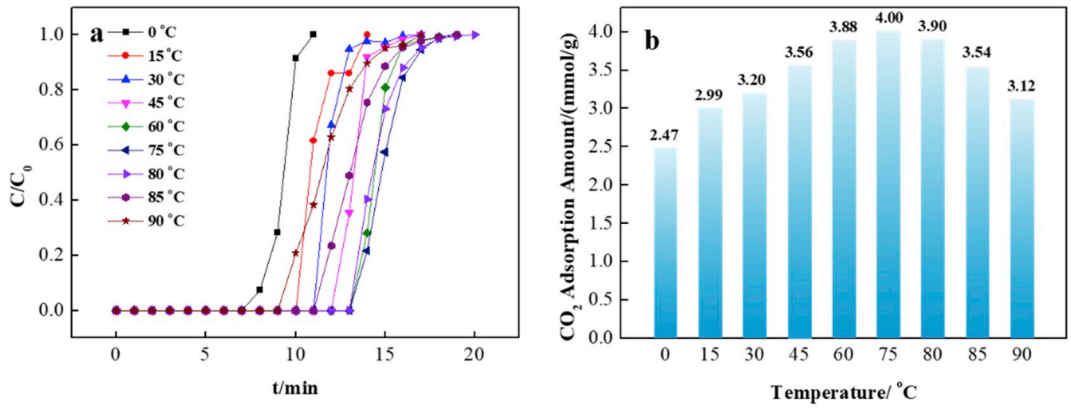

Fig. 7. a) Breakthrough curves of CO_2 adsorption, and b) CO_2 adsorption amounts of SSBA-15-PEI(600) under various temperature. (CO_2/N_2 ratio was 1:4; gas flow rate was 30 mL/min).

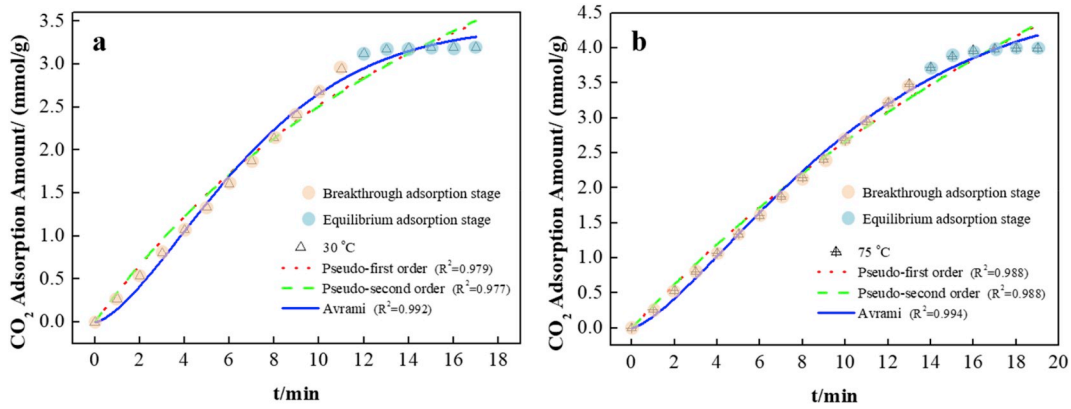

Fig. 8. The corresponding fits of experimental data on CO_2 adsorption amount of SSBA-15-PEI(600) with three kinetic models at a) 30 °C, and b) 75 °C.

$$q_t = q_e - q_e \frac{6}{\pi^2} e^{\frac{-\pi^2 k_f t}{15}} \quad (4)$$

Intraparticle diffusion model (Weber-Morris plot):

$$q_t = k_{id} t^{1/2} + C \quad (5)$$

Boyd's film-diffusion model:

$$B_t = \left(\sqrt{\pi} - \sqrt{\pi - \frac{\pi^2 F}{3}} \right)^2 \quad (F < 0.85) \quad (6)$$

$$B_t = -0.4977 - \ln(1 - F) \quad (F > 0.85) \quad (7)$$

where $F = \frac{q_t}{q_e}$.

The adsorption of CO_2 on SSBA-15-PEI(600) was not influenced by simple film-diffusion nor interparticle diffusion, as the B_t did not vary linearly with the time (Fig. S8, Supplementary Information) and the simulative curves of interparticle diffusion model lacked of fit with the experimental data (Fig. S9, Supplementary Information) [45]. Hence, the intraparticle diffusion model was applied to predict the rate-controlling step of SSBA-15-PEI(600) at all temperatures. As shown in Fig. 9, the three mode-linearity appeared and the adsorption process could be divided into three stages: the external adsorption stage (boundary layer diffusion), the gradual adsorption stage (intraparticle diffusion), and the equilibrium stage. The first stage presented the

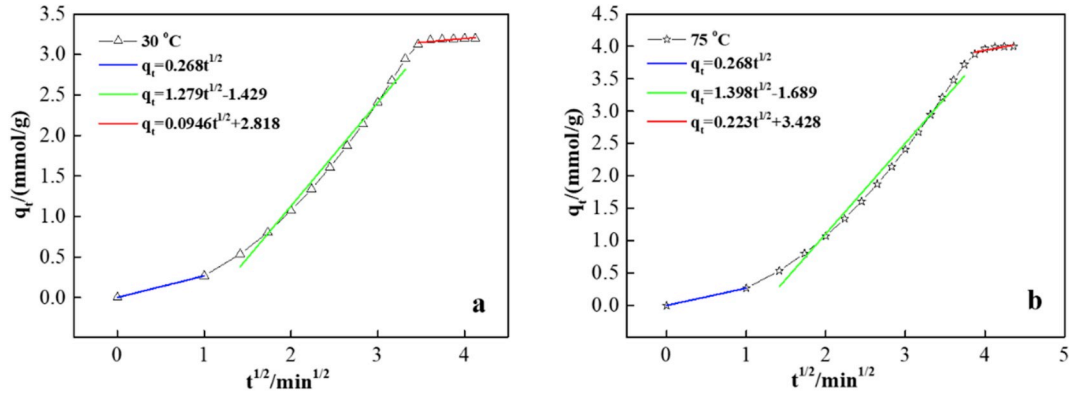

Fig. 9. Weber-Morris plot of CO_2 adsorption over SSBA-15-PEI(600) at a) 30 °C, and b) 75 °C.

minimum slope at 0 °C and 15 °C (Figs. S10a and b, and Table S5, Supplementary Information), indicating that the boundary layer diffusion process was the rate-controlling step at low temperature. When the temperature was over 30 °C, the surface reaction of equilibrium stage became the rate-controlling step since the minimum slope appeared at the third stage (Fig. S10, and Table S5, Supplementary Information). Overall, the second stage, as was gradual adsorption stage, presented the fastest adsorption rate during the whole adsorption process, indicating that the micro-mesoporous structure of SSBA-15-PEI(600) is favorable for the intraparticle diffusion of CO_2 molecules, in which short mesochannnels and structural mesopores facilitated CO_2 diffusion inside mesochannels, and abundant intrawall micropores benefited CO_2 diffusion between mesochannels.

5. Conclusions

In summary, the well-ordered hexagonal SBA-15 with short mesochannels was successfully prepared via an innovative non-hydrothermal method which used $NH_3 \cdot H_2O$ as catalyst instead, and this new method has been proven to synthesis conventional SBA-15 consists of rope-like particles. SSBA-15 prepared under the optimum condition (30 min of ripening time and 25% of $NH_3 \cdot H_2O$ concentration) consisted of cuboid-like particles, had mesochannel length of 250 ± 50 nm and structural mesopore size of 9.8 nm, and importantly, required less than 40 min to form a well-ordered framework, which is time and energy saving by abolishing hydrothermal process. The application in CO_2 adsorption and investigations on the kinetics and diffusion models demonstrated that solid amine adsorbents based on as-prepared SSBA-15 possess well properties as are excellent regeneration ability, fast kinetics and high adsorption capacity, and are favorable for intraparticle diffusion of CO_2 molecules, which could be attributed to the unique micro-mesoporous structure and short mesochannel length of SSBA-15. We believe that this innovative $NH_3 \cdot H_2O$ catalysis strategy will inspire the efficient synthesis of other materials which require hydrothermal process.

Declaration of competing interest

The authors declare that they have no known competing financial interests or personal relationships that could have appeared to influence the work reported in this paper.

CRediT authorship contribution statement

Beibei Ma: Conceptualization, Methodology, Software, Formal analysis, Investigation, Data curation, Writing - original draft, Visualization. **Rijia Lin:** Visualization, Writing - review & editing. **Hui He:** Validation, Resources, Visualization. **Qinghua Wu:** Software, Resources. **Shuixia Chen:** Supervision, Conceptualization, Writing - review & editing.

Acknowledgements

The authors gratefully acknowledge the financial support provided by the National Natural Science Foundation of China (Grant No. 51873238), Science and Technology Project of Guangdong Province (2017B090915001).

Appendix A. Supplementary data

Supplementary data to this article can be found online at https://doi.org/10.1016/j.compositesb.2020.107782.

References

[1] Kresge C, Leonowicz M, Roth W, Vartuli J, Beck J. Ordered mesoporous molecular sieves synthesized by a liquid-crystal template mechanism. Nature 1992;359:710–2.
[2] Meysam N, Dawood E. Ionic liquid-modified magnetic mesoporous silica supported tungstate: a powerful and magnetically recoverable nanocatalyst. Compos B Eng 2019;176:107308.
[3] Zahra R, Dawood E, Meysam N, Reza M. Magnetic mesoporous MCM-41 supported boric acid: a novel, efficient and ecofriendly nanocomposite. Compos B Eng 2019;164:10–7.
[4] Fatemeh R, Fatemeh F, Rafael L. Cytosine-functionalized SBA-15 mesoporous nanomaterials: synthesis, characterization and catalytic applications. Microporous Mesoporous Mater 2017;253:64–70.
[5] Bennadja Y, Beaunier P, Margolese D, Davidson A. Fine tuning of the interaction between Pluronic surfactants and silica walls in SBA-15 nanostructured materials. Microporous Mesoporous Mater 2001;44–45(6):147–52.
[6] Karlsson A, Stöcker M, Schmidt R. Composites of micro- and mesoporous materials: simultaneous syntheses of MFI/MCM-41 like phases by a mixed template approach. Microporous Mesoporous Mater 1999;27(2–3):181–92.
[7] Lee J, Park Y, Kim P, Kim H, Yi J. Single-step preparation of Ni catalysts supported on mesoporous silicas (SBA-15 and SBA-16) and the effect of pore structure on the selective hydrodechlorination of 1,1,2-trichloroethane to VCM. J Mater Chem 2004;97(2–3):195–203.
[8] Voort PVD, Ravikovitch PI, Jong KPD, Benjelloun M, Bavel EV, Janssen AH, Neimark AV, Weckhuysen BM, Vansant EF. Plugged hexagonal mesoporous templated silica: a unique micro- and mesoporous material with internal silica nanocapsules. J Phys Chem B 2002;141:45–52.
[9] Tang F, Li L, Chen D. Mesoporous silica nanoparticles: synthesis, biocompatibility and drug delivery. Adv Mater 2012;24:1504–34.
[10] Wang Y, Zhao Q, Han N, Bai L, Li J, Liu J, Wang S. Mesoporous silica nanoparticles in drug delivery and biomedical applications. Nanomed Nanotechnol Biol Med 2015;11(2):313–27.
[11] Mariana S, Sonia M, Damian P, Maria LM, Isabel S. Environmental chiral analysis of β-blockers: evaluation of different n-alkyl-modified SBA-15 mesoporous silicas as sorbents in solid-phase extraction. Environ Chem 2018;15(6):362–71.
[12] Nattawut O, Chaianun P, Narongrit S, Krittanun D, Chalermpan K, Wina R, Narong C, Juthamas J, Sanchai P, Jatuporn W. Characterization and comprehension of zeolite NaY/mesoporous SBA-15 composite as adsorbent for paraquat. Mater Chem Phys 2017;193:470–6.
[13] Sarah R, Michael T. Influence of temperature and high-pressure on the adsorption behavior of $scCO_2$ on MCM-41 and SBA-15. J Supercrit Fluids 2019;144:122–33.
[14] Younsang B, Bong JC, Suyoung M, Jeong HK, Jinsoo K. Highly CO selective Cu(I)-doped MIL-100(Fe) adsorbent with high CO/CO_2 selectivity due to π complexation: effects of Cu(I) loading and activation temperature. Microporous Mesoporous Mater 2019;274:17–24.
[15] Wang L, Zhang L, Li H, Ma Y, Zhang R. High selective production of 5-hydroxymethylfurfural from fructose by sulfonic acid functionalized SBA-15 catalyst. Compos B Eng 2019;156:88–94.
[16] Cheng X, Wang D, Liu J, Kang X, Yan H, Wu A, Gu Y, Tian C, Fu H. Ultra-small Mo_2N on SBA-15 as a highly efficient promoter of low-loading Pd for catalytic hydrogenation. Nanoscale 2018;10:22348–56.
[17] Rory H, Charles M, James AS. Co-SBA-15 catalysts in the hydrolysis of NH_3BH_3 - influences of Co precursors and catalyst pre-treatment. Catal Commun 2018;107:14–7.
[18] Ruiyun L, Heyuan S, Guoqin W, Jing C. Efficient and reusable SBA-15-immobilized Brønsted acidic ionic liquid for the ketalization of cyclohexanone with glycol. RSC Adv 2018;8:7179–85.
[19] Yayati NP, Kaiprathu A, Ayyamperumal S, Maqsood A, Dhanjay S, Sushant KB. Cerium ions grafted on functionalized mesoporous SBA-15 molecular sieves: preparation and its catalytic activity on p-cresol oxidation. Catal Lett 2018;148(1):465–73.
[20] Zhang H, Sun JM, Ma D. Unusual mesoporous SBA-15 with parallel channels running along the short axis. J Am Chem Soc 2004;126(24):7440–1.
[21] Chen SY, Tang CY, Chuang WT, Lee JJ, Tsai YL, Chan JCC, Lin CY, Liu YC, Cheng S. A facile route to synthesizing functionalized mesoporous SBA-15 materials with platelet morphology and short mesochannels. Chem Mater 2008;20:3906–16.
[22] Linton P, Wennerstrom H, Alfredsson V. Controlling particle morphology and size in the synthesis of mesoporous SBA-15 materials. Phys Chem Chem Phys 2010;12(15):3852–8.
[23] Yu C, Tian B, Fan J, Stucky GD, Zhao D. Morphology development of mesoporous materials: a colloidal phase separation mechanism. Chem Mater 2004;16(5):889–98.
[24] Cyril P, Karen W, Adam FL. An energy-efficient route to the rapid synthesis of organically-modified SBA-15 via ultrasonic template removal. Green Chem 2014;16:197–202.
[25] Pirez C, Morin JC, Manayil JC, Lee AF, Wilson K. Sol-gel synthesis of SBA-15: impact of HCl on surface chemistry. Microporous Mesoporous Mater 2018;271:196–202.
[26] Dharitri R, Surjyakanta R, Parida KM. Organic amine-functionalized silica-based mesoporous materials: an update of syntheses and catalytic applications. RSC Adv 2014;4:57111–24.
[27] Murad G, Tompsett GA, Conner WC, Yngvesson KS. Microwave synthesis of SAPO-11 and AlPO-11: aspects of reactor engineering. ChemPhysChem 2008;9(17):2580–91.

[28] Schiel MA, Domini CE, Chopa AB, Silbestri GF. Microwave-assisted syntheses of thiophene-based ionic liquids: structural design and optimization. Synethsis 2018; 50(24):4846–54.
[29] Rezayati S, Hajinasiri R, Erfani Z. Microwave-assisted green synthesis of 1,1-diacetates (acylals) using selectfluor™ as an environmental-friendly catalyst under solvent-free conditions. Res Chem Intermed 2016;42(3):2567–76.
[30] Ma B, Zhuang L, Chen S. Rapid synthesis of tunable-structured short-pore SBA-15 and its application on CO_2 capture. J Porous Mater 2016;23:529–37.
[31] Celer EB, Jaroniec M. Temperature-programmed microwave-assisted synthesis of SBA-15 ordered mesoporous silica. J Am Chem Soc 2006;128(44):14408–14.
[32] Zhuang L, Ma B, Chen S, Hou X, Chen S. Fast synthesis of mesoporous silica materials via simple organic compounds templated sol-gel route in the absence of hydrogen bond. Microporous Mesoporous Mater 2015;213:22–9.
[33] Lei C, Hu Z, Zhang Y, Yang H, Li J, Hu S. Tailoring structural and physical properties of polymethylsilsesquioxane aerogels by adjusting $NH_3{\bullet}H_2O$ concentration. Microporous Mesoporous Mater 2018;258:236–43.
[34] Liu X, Rong W, Liu X, Ren X, Chen J, Zhu Y. Preparation of cerium dioxide film by anodization in $Na_2C_2O_4$-$NH_3{\cdot}H_2O$-H_2O-$(CH_2OH)_2$ electrolyte. Adv Mater Eng 2017;748:7–11.
[35] Jiang C, Sun X. Stability of emulsion liquid membrane and membrane phase reaction spectrum study of $NH_3{\cdot}H_2O$ system. Desalin Water Treat 2016;57(41): 19112–20.
[36] Aliakbar H-G, Yang Y, Abdelhamid S. Effect of the pore length on CO_2 adsorption over amine-modified mesoporous silicas. Energy Fuel 2011;25:4206–10.
[37] He H, Hu Y, Chen S, Zhuang L, Ma B, Wu Q. Preparation and properties of a hyperbranch-structured polyamine adsorbent for carbon dioxide capture. Sci Rep 2017;7(1):3913–23.
[38] Sing KSW, Everett DH, Haul RAW, Moscou L, Pierotti RA, Rouquerol J, Siemieniewska T. Reporting physisorption data for gas/solid systems with special reference to the determination of surface area and porosity. Pure Appl Chem 1984; 57:603–19.
[39] He Z, Junming S, Ding M, Gisela W, Dang SS, Xinhe B. Engineered complex emulsion system: toward modulating the pore length and morphological architecture of mesoporous silicas. J Phys Chem B 2006;110:25908–15.
[40] Zholobenko VL, Khodakov AY, Durand D. Impact of aqueous impregnation on the long-range ordering and mesoporous structure of cobalt containing MCM-41 and SBA-15 materials. Microporous Mesoporous Mater 2003;66:297–302.
[41] Zhang H, Wang B, Feng A, Zhang N, Jia Z, Huang Z, Liu X, Wu G. Mesoporous carbon hollow microspheres with tunable pore size and shell thickness as efficient electromagnetic wave absorbers. Compos B Eng 2019;167:690–9.
[42] Zhuang L, Chen S, Lin R, Xu X. Preparation of a solid amine adsorbent based on polypropylene fiber and its performance for CO_2 capture. J Mater Res 2013;28(20): 2881–9.
[43] Lin R, Zhuang L, Xu X, Chen S. Design of a viscose based solid amine fiber: effect of its chemical structure on adsorption properties for carbon dioxide. J Colloid Interface Sci 2013;407:425–31.
[44] Wang X, Guo Q, Kong T. Tetraethylenepentamine-modified MCM-41/silica gel with hierarchical mesoporous structure for CO_2 capture. Chem Eng J 2015;273: 472–80.
[45] Loganathan S, Tikmani M, Edubilli S, Mishra A, Ghoshal AK. CO_2 adsorption kinetics on mesoporous silica under wide range of pressure and temperature. Chem Eng J 2014;256:1–8.